JOURNAL OF AIRCRAFT
Vol. 32, No. 3, May–June 1995

Analysis of Some Interference Effects in a Transonic Wind Tunnel

Giovanni Lombardi*
University of Pisa, Pisa 56126, Italy
and
Mauro Morelli†
Council for Scientific and Industrial Research, Pretoria 0001, South Africa

The effects of the walls of a test section on a model in transonic flow were investigated by using the AGARD Calibration Model B. Tests were carried out in a closed-circuit pressurized tunnel, with a confined square test section of 1.5 m width, with tapered slots giving a 5% porosity. Two models with different dimensions were used, with 0.85 and 0.056% blockage ratios. Longitudinal aerodynamic characteristics were analyzed by means of measurements performed at varying angles of attack (up to 24 deg) and Mach numbers from 0.3 to 1.2. In some flow conditions wall interference effects were probably present. However, the forces and moments dependent on the pressure distribution were likely to be related to the same factors, and therefore, the above effects tended to disappear when longitudinal stability and lift-dependent drag were analyzed as a function of lift characteristics. The drag rise Mach number evaluation seems be fully free from blockage effects. The dimensions of the tested larger model can be considered to be the largest reasonable ones for industrial applications, but, probably, not sufficiently small when high accuracy is required.

Nomenclature

b = model span, Fig. 1, mm
C_D = forebody drag coefficient
$C_{D\min}$ = minimum value for C_D for a given Mach number
C_{D0} = zero-lift drag coefficient for a given Mach number
C_L = forebody lift coefficient
C_M = forebody pitching moment coefficient
c_b = chord at the body-wing junction, Fig. 1, mm
c_{ma} = mean aerodynamic chord, mm
c_r = root chord, Fig. 1, mm
D = model fuselage diameter, Fig. 1, mm
d = diameter of the support sting, mm
K = coefficient in the relation $C_D = D_{D0} + KC_L^2$
L_a = base to wing trailing-edge distance, Fig. 1, mm
L_f = ogive length, Fig. 1, mm
L_t = total length, Fig. 1, mm
M = Mach number
$\bar{M}$ = static pipe average Mach number
M_P = pseudo-Mach number calculated from the equilibrium plenum pressure
P = confidence level
S_w = gross wing area, Fig. 1, mm^2
w = test section width, mm
x = streamwise coordinate in the test section, Fig. 2, mm
x_{ref} = distance of the moment reference point from the model base, Fig. 1, mm
α = angle of attack, deg

Introduction

THE interference on the flowfield around a model caused by wind-tunnel walls is known to be one of the main sources of error affecting the accuracy of experimental data. The classical correction criteria are not satisfactory for an accurate data correction, being based on insufficiently representative theoretical linear models,[1] whose validity is limited to low velocities and angles of attack; however, even in these conditions, the accuracy of these criteria is not high since they do not account for physical tunnel characteristics (i.e., fillets, re-entry doors, etc.[2]). With the introduction of the ventilated test section for high-speed subsonic and transonic testing, new procedures have been devised to extend the classical wall interference methods for correcting model test data. Because of the complex nature of the interference, a satisfactory general analytical solution to this problem for ventilated walls is far from being achieved. More recently, new correction methods were introduced, based on more complex procedures, coupling measurements—typically pressure and/or velocity on the wall or in the field—with numerical calculations.[3,4] Anyway, these procedures experience difficulties because of the small quantities to be measured, the uncertainty of the devices used to make the measurements and the interference from other sources,[2] as well as because of the complexity of flow calculation. Furthermore, in three-dimensional problems, the number of field measurements necessary for a proper wall correction evaluation is so large that it yields an experimental procedure very difficult to perform, at least regarding industrial applications. This is particularly true for transonic conditions or for high angles of attack, because linear models are not valid and it is almost impossible to use a reliable numerical code.

The above considerations explain why limiting model dimensions as much as possible remains the best way to avoid unacceptable errors. On the other hand, the importance of testing the largest possible model is evident, not only to maximize the Reynolds number but, especially, to improve the accuracy of force measurement and of the model itself.[5] Thus, it is important to have reliable criteria for choosing model size[6]; advancing knowledge on this matter is the main purpose of the present research activity.

The effects of the walls of the wind tunnel on a model in transonic flow were investigated by using the AGARD Calibration Model B specified in Ref. 7 (see Fig. 1). It is an

Received March 26, 1994; revision received Aug. 31, 1994; accepted for publication Aug. 31, 1994.

*Assistant Professor, Department of Aerospace Engineering, Via Diotisalvi, 2. Member AIAA.
†Research Engineer, Medium Speed Wind Tunnel, P.O. Box 395.

ogive-cylinder body with a delta wing having a symmetrical circular arc airfoil section, already tested in many different wind tunnels.[8] Two models with different dimensions were used. The first one (named "large" model) had a nominal diameter (Fig. 1) $D = 150$ mm, with a corresponding blockage at zero angle of attack of 0.85% (including the wing-sectional area), and a model-to-test section width ratio b/w of 0.400. The other one (named "small" model) had a nominal diameter $D = 38.5$ mm, with a corresponding blockage of 0.056% and a b/w ratio of 0.103. Because of the very low blockage of the small model, the latter could be considered actually free of wall interference. The dimensions of the large model were chosen as indicative of the largest possible for the test section geometry.[9]

To avoid differences caused by different flow characteristics, which may significantly affect forces (particularly, the turbulence scale and intensity[10]), the test conditions were kept the same for both models; in this way the two models were tested at different Reynolds numbers, but this influence can be considered to be (at least qualitatively) known, particularly for the tested model, which had been extensively studied in many different conditions.[8,11]

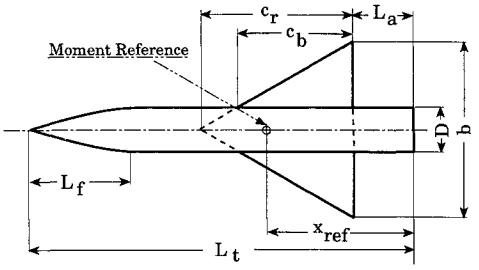

Nominal dimensions			
L_t	= 8.5 D	x_{ref}	= 3.148 D
L_f	= 3 D	c_b	= 2.598 D
L_a	= 1.402 D	b	= 4 D

Gross wing area $S_W = (b \times c_r)/2$

Fig. 1 AGARD B model.

Experimental Setup

Tests were carried out in the Medium Speed Wind Tunnel of the CSIR Laboratories, in South Africa. This is a closed-circuit variable density transonic wind tunnel. Its operational speed ranges from $M = 0.25$ to 1.5, with pressure varying from 20 to 250 kPa; Reynolds number can be changed by modifying the pressure. The test section has a 1.5×1.5 m^2 cross section, 4.5 m in length. All four walls are equally longitudinally slotted ("coke bottle" type) for a total porosity of 5%, following the scheme in Fig. 2; the lateral walls are parallel, while the upper and lower ones are slightly diverging, 0.7 deg each, starting from the test section inlet.

The main flow characteristics in the test section are summarized in Table 1, derived from the complete calibration of the wind tunnel.[12]

The models were assembled on the main model support (Fig. 3), which consists of a pitch sector with a roll head that transmits the attitude movements to the model. They were connected through internal balances onto a sting, and base pressure probes were fitted onto both models. On the large model two pressure orifices were fitted in diametrically opposite positions on the sting at the base of the model, whereas on the small model a single orifice was used to measure the base pressure. The base axial force coefficient was evaluated by calculating the pressure acting on the model base area, this value was subtracted from the measured axial force coefficient to determine the forebody axial force coefficient,[11] which was used to evaluate the forebody drag and lift coefficients C_D and C_L.

The mounting scheme is identical for the two models, in particular the sting diameter to base diameter ratio d/D for the large model is 0.500, and for the small model it is 0.506. Two internal, six component strain gauge balances were used to measure the forces on the models; the balances were calibrated with a second-order matrix technique.

The two models were positioned in the same zone of the wind-tunnel test section; the large model between the stations $x = 2213$–3488 (Fig. 2), the small model between the stations $x = 2620$–2948. Both models were stationed in the "standard test section" as defined by the primary tunnel calibration,[13] namely from $x = 2100$ to 3600. Consequently, the tunnel Mach number determination is obtained from the offset parameter $(\bar{M} - M_p)$ calculated during the static pipe correlation where the value of $\bar{M}$ is calculated across the standard test section.

Both models were tested under the same environmental conditions and attitudes, namely, from $M = 0.3$ to 0.9 in 0.1

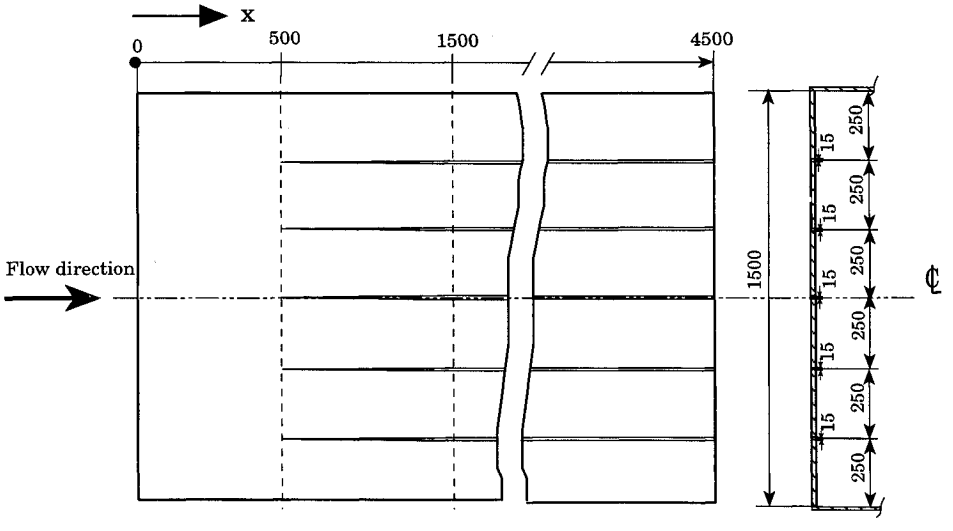

Fig. 2 Definition of the walls of the wind-tunnel test section. The slots on the four walls are positioned in the same way (all dimensions are in millimeters).

Table 1 Main flow characteristics in the wind-tunnel test section

Stability of Mach number with time	$\sigma_{M_t} \leq 0.0014$
Stability of stagnation pressure with time	$\sigma_{P_0} \leq 0.0012$ KPa
Stability of stagnation temperature with time	$\sigma_{T_0} \leq 2$ K
Humidity level dewpoint	2 deg below tunnel static temperature
Spatial variation of Mach number	$\sigma_M \leq 0.002$ (subsonic)
	$\sigma_M \leq 0.004$ (supersonic)
Spatial variation of flow angularity	$\sigma_\mu \leq 0.15$ deg (subsonic)
	$\sigma_\mu \leq 0.30$ deg (supersonic)
Acoustic pressure coefficient fluctuation	$\Delta c_p \leq 0.01$
Acoustic fluctuation frequency content	$[nF(n)]^{1/2} \leq 0.007$
Turbulence level	$\sigma_u/U_\infty \leq 0.001$ (low Mach)
	$\sigma_u/U_\infty \leq 0.002$ (high Mach)

σ = root mean square.

Table 2 Nominal and real dimensions of the two models

	Large model		Small model	
	Nominal	Real	Nominal	Real
D	150	150	38.5	38.5
L_t	1275	1274.70	327.5	328.44
b	600	598.68	154	152.45
c_b	389.7	389.30	100.03	100.00
L_a	210.3	210.20	53.98	54.05
c_r	—	519.60	—	133.36
c_{ma}	—	346.4	—	89.0
x_{ref}	—	472.2	—	121.2
S_w	—	155,537.1	—	10,165.7
Wetted wing area, mm^2	—	89,354.6	—	5,185.0
Model volume, m^3	—	0.0172	—	0.000291
Blockage factor at α = 0 deg	—	0.850%	—	0.056%
Blockage factor at α = 24 deg	—	4.66%	—	0.30%
b/w	—	0.400	—	0.103
d/D	—	0.500	—	0.506

Variables refer to Fig. 1.

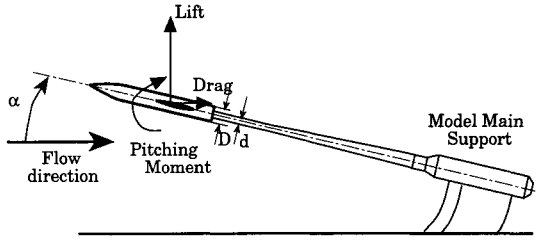

Fig. 3 Scheme of the support and reference system.

steps, from $M = 0.95$ to 1.1 in 0.05 steps, and at $M = 1.2$. Auxiliary suction was used at Mach numbers between 0.9–1.2. The mass flow evacuated from the test section was 2% of the plenum evacuation system (PES) for $M = 0.9$–1.1, and 2.5% of the PES at $M = 1.2$.

Under the tested conditions the Reynolds number, referred to the model total length L_t, varied from 9.2×10^6 to 1.7×10^7 for the large model, and from 2.4×10^6 to 4.5×10^6 for the small model.

The models were tested at pitch angles that ranged from −4 to 24 deg for Mach numbers up to 0.7, and from −4 to 17.5 deg for the remaining Mach numbers. In these conditions no model oscillation was detected during the angle-of-attack sweep for either model. The measured body axis forces were converted into drag and lift values, and the effects of the base pressure were eliminated, i.e., only the forces acting on the forebody were considered.

The balance data were acquired through a NEFF system 620 series 500 provided with a 16-bit A/D converter. The pressure data were acquired through a Scanivalve 20 C system with a 12-bit A/D converter.

The adopted reference system is shown in Fig. 3. The force coefficients were nondimensionalized with the dynamic pressure and the gross wing area (S_w, including the wing carry through the fuselage, see Fig. 1), the moment coefficients with the dynamic pressure, the gross wing area and the mean aerodynamic chord (c_{ma}) and were referred to the quarter-chord point of the mean aerodynamic chord.

The quality control inspection carried out on the models is fully described in Ref. 14; it was accomplished on a model 2202 DEA IOTA coordinate measuring machine with computerized measuring and recording capability. In Table 2 the nominal and real dimensions of the two models are reported, the uncertainty in the linear measurements being less than 0.01 mm.

An automatic Mach controller maintained a constant Mach number, compensating for Mach number variations such as those induced by the model pitch cycle. The uncertainty in Mach number was 0.002[15]; that in the angle-of-attack positioning was less than 0.1 deg, and data were corrected for sting deflections.

In Table 3, for the large model, the total uncertainties in the data that can be attributed to instrumentation errors (forces, dynamic pressure, and base pressure measurements), reference dimension evaluation (surfaces, lengths, and moment reduction points), and data acquisition procedure are shown and expressed as coefficient uncertainty; the small model uncertainties are of the same order and are reported in Ref. 16. In Table 4 the uncertainties in the zero-lift drag coefficient evaluation are shown. The uncertainties were determined as suggested in Ref. 17, for a confidence level of 95%. It has to be noted that because of the use of the wind tunnel under identical flow conditions (for a given Mach number), the bias uncertainty should not be considered in its entirety when comparing the two models, because it includes a fraction (that dependent on flow measurements and on the evaluation of the model dimensions) that was the same in both cases. For this reason the bias error is reported both as total values and

Table 3 Bias and precision uncertainty level in the force coefficients evaluation procedure (P = 0.95), large model

	Lift coefficient								
	0.1			0.6			1.1		
M	Balance bias	Total bias	Precision	Balance bias	Total bias	Precision	Balance bias	Total bias	Precision
0.3	0.0041	0.0073	0.0019	0.0041	0.0068	0.0016	0.0041	0.0063	0.0015
1.0	0.0013	0.0038	0.0015	0.0013	0.0031	0.0012	0.0013	0.0028	0.0011
1.2	0.0011	0.0028	0.0013	0.0011	0.0025	0.0010	0.0011	0.0023	0.0009
	Pitching moment coefficient								
	0.02			0.07			0.12		
M	Balance bias	Total bias	Precision	Balance bias	Total bias	Precision	Balance bias	Total bias	Precision
0.3	0.00072	0.00188	0.00042	0.00072	0.00178	0.00038	0.00072	0.00172	0.00033
1.0	0.00020	0.00061	0.00036	0.00020	0.00057	0.00032	0.00020	0.00053	0.00028
1.2	0.00017	0.00054	0.00031	0.00017	0.00046	0.00024	0.00017	0.00041	0.00021
	Drag coefficient								
	0.1			0.2			0.3		
M	Balance bias	Total bias	Precision	Balance bias	Total bias	Precision	Balance bias	Total bias	Precision
0.3	0.0046	0.0078	0.0021	0.0046	0.0074	0.0016	0.0046	0.0069	0.0014
1.0	0.0017	0.0042	0.0016	0.0017	0.0036	0.0015	0.0017	0.0032	0.0012
1.2	0.0013	0.0031	0.0015	0.0013	0.0028	0.0012	0.0013	0.0025	0.0012

Table 4 Bias and precision uncertainty level in the C_{D_0} measurement procedure (P = 0.95)

	Large model			Small model		
M	Balance bias	Total bias	Precision	Balance bias	Total bias	Precision
0.3	0.0031	0.0046	0.0019	0.0033	0.0045	0.0025
1.0	0.0011	0.0029	0.0013	0.0014	0.0029	0.0018
1.2	0.0009	0.0024	0.0011	0.0011	0.0025	0.0015

as balance bias; however, only the latter gives the uncertainty in the comparisons.

Analysis of the Results

Preliminary tests performed at different Reynolds numbers showed that no significant effects of this parameter were present, especially on the pressure-dependent forces; this was probably a consequence of the model geometry, characterized by a delta wing (the more so as it was small compared with the body dimensions). This confirms previous results obtained in other wind tunnels.[8-11] Comparisons with previous data were very satisfactory,[13] but are beyond the scope of the present article and are not discussed here.

In a subsonic regime, C_L-α curves do not appear to be affected by blockage effects, as can be seen by analyzing, e.g., Fig. 4a (M = 0.3). In the transonic regime, differences are, again, very small at low angles of attack (up to 10 degs), whereas more pronounced differences appear for higher angles of attack; this behavior was found for M = 0.8–0.9 (Figs. 4b and 4c), whereas for M = 1 and 1.05 (Figs. 4d and 4e) the behavior was different. Small differences were observed at any considered angle of attack that was of the same order as measurement uncertainty, and therefore, did not evidence any blockage effect on lift characteristics when crossing to sonic freestream conditions. Any difference disappeared, at the investigated angles of attack, at supersonic freestream, as shown in Fig. 4f (M = 1.2). Thus, it appeared that at high angles of attack, in a low transonic regime, significant blockage effects were present on lift characteristics, while less important effects were present from M = 0.95 to 1.1, effects that tended to disappear as the Mach number increased.

However, it is very interesting to note that the effects on lift were strongly correlated with those on the pitching moment. Figure 5 shows the moment coefficient C_M vs C_L for the Mach numbers previously considered; only very localized differences can be observed, corresponding to the inflexion point in the curves, and, furthermore, they are particularly prominent at the lower Mach numbers. Since measurement uncertainty is higher in a subsonic regime (Table 3) because forces are smaller, it is then possible that such differences are derived from measurement uncertainty, which is known to be particularly important in moment evaluation. The correlation between lift and pitching moment is confirmed by analyzing Fig. 6, which shows, e.g., the variation of the C_M/C_L ratios with the Mach number for angles of attack of 8 and 17.5 deg: the curves are almost perfectly superimposable, except in the subsonic regime, where some differences are present. It is therefore very probable that blockage effects on moment evaluation were present, but they had the same origins as those related to the lift ones, which is why they disappear when longitudinal stability is studied as a function of lift characteristics. As to the low subsonic regime, no definite conclusions can be achieved, because the differences in the two model measurements are not large enough to be surely attributable to blockage effects.

Drag characteristics can be analyzed as zero-lift drag and lift-dependent drag. The lift-dependent drag (Fig. 7) shows, for any Mach number, a very surprising coincidence for the

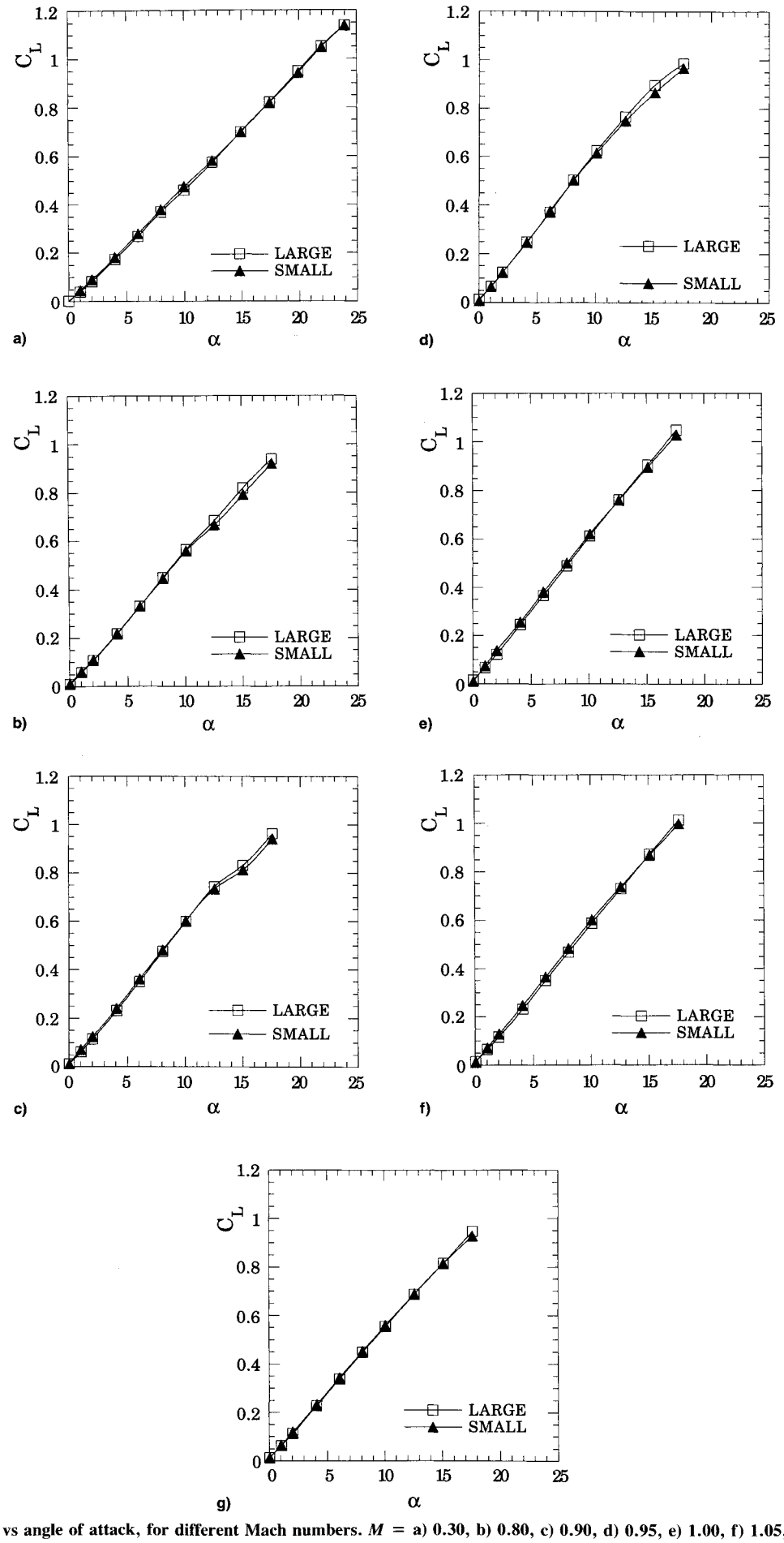

Fig. 4 Lift vs angle of attack, for different Mach numbers. M = a) 0.30, b) 0.80, c) 0.90, d) 0.95, e) 1.00, f) 1.05, and g) 1.20.

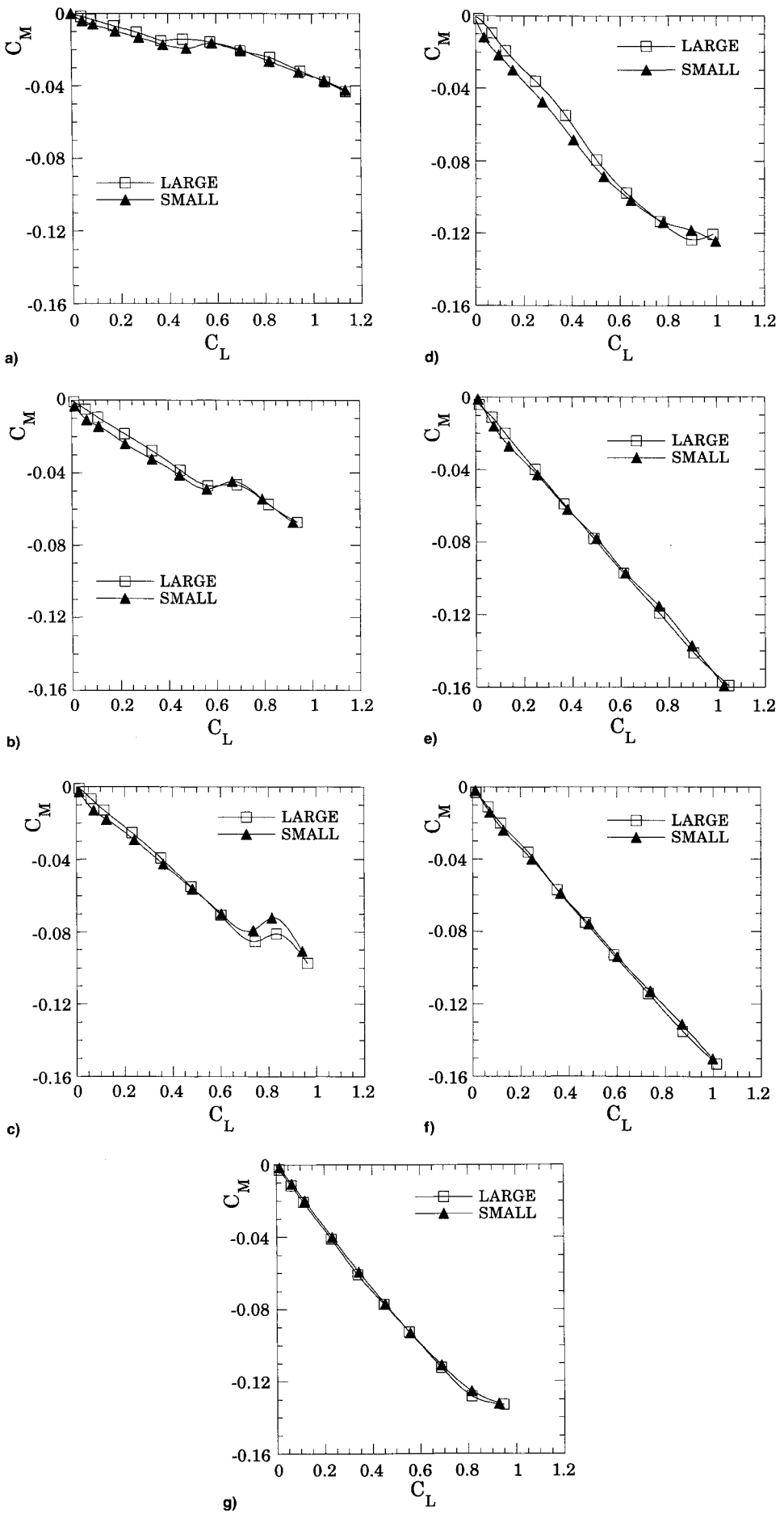

Fig. 5 Pitching moment vs lift, for different Mach numbers. M = a) 0.30, b) 0.80, c) 0.90, d) 0.95, e) 1.00, f) 1.05, and g) 1.20.

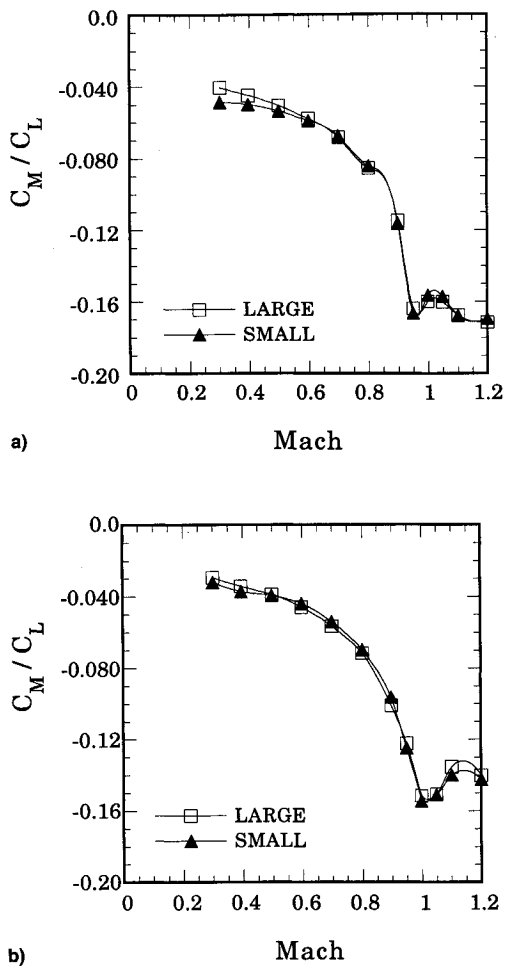

Fig. 6 Pitching moment to lift ratios vs Mach number, for different angles of attack. α = a) 8.0 and b) 17.5 deg.

two models, also characterized by an almost linear correlation between the C_L^2 and the $C_D - C_{D\min}$ values. In Fig. 8 the least-square best-fit interpolated linear coefficient K between C_L^2 and $C_D - C_{D0}$ is reported (because the symmetry of the body is $C_{D\min} = C_{D0}$) as a function of the Mach number; differences are almost negligible, and there are very high values of the correlation factor, in any case higher than 0.995. Even in this setting, blockage effects are likely to occur when changing the angle of attack, but again, they have the same origins as those related to lift, which is why they disappear when drag (as is usually the case) is studied as a function of lift.

The zero-lift drag is difficult to measure because of the small values of the forces involved, with a consequently high error level (Table 4); an accurate analysis of the zero-lift drag characteristics would require a different test campaign, with a completely different choice of test procedures. In Fig. 9 the C_{D0}, as a function of the Mach number, is shown; differences are present, but they may be due to a Reynolds number effect (in this case, a greater extent of laminar flow on the small model, affecting results in the way previously shown): indeed, this parameter is markedly affected by viscosity. In any case, differences are of the (high, in this case) uncertainty order, except for the higher Mach number where differences are more important, being significantly higher than the uncertainty level. Thus, it is likely that, in supersonic flow conditions, a blockage effect affecting zero drag measurements was present, while no definite conclusions are possible with respect to the other flow conditions. However, it is of interest that the evaluation of the drag rise Mach number does not appear to be affected by model scale (Fig. 9).

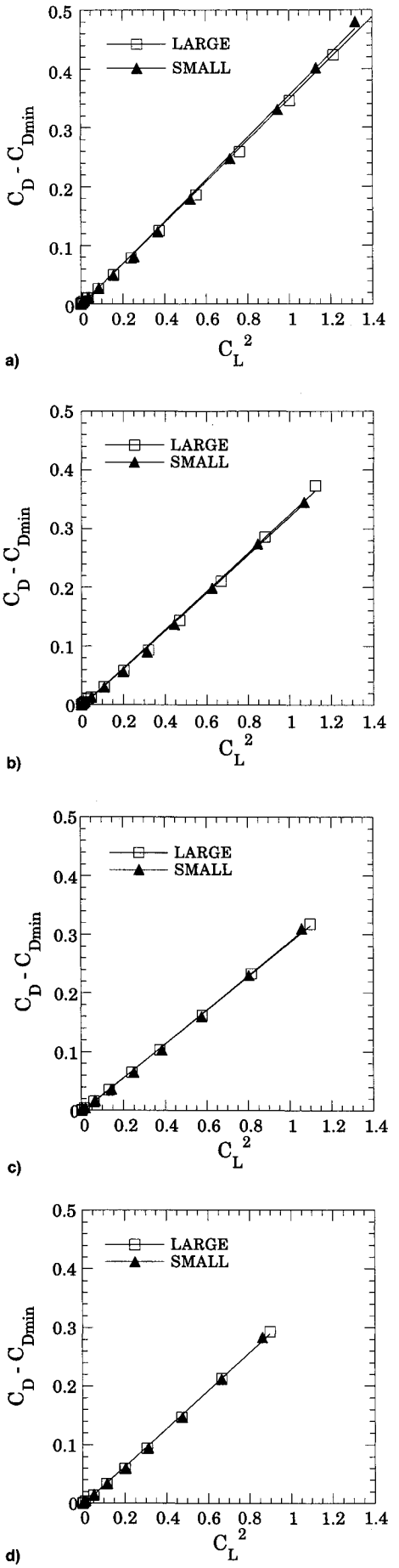

Fig. 7 Drag, zero-lift drag vs squared lift, for different Mach numbers. M = a) 0.5, b) 0.8, c) 1.0, and d) 1.2.

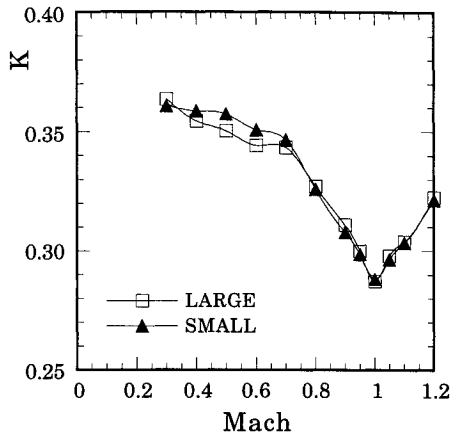

Fig. 8 Linear K coefficient, relating incremental drag to squared lift, vs Mach number.

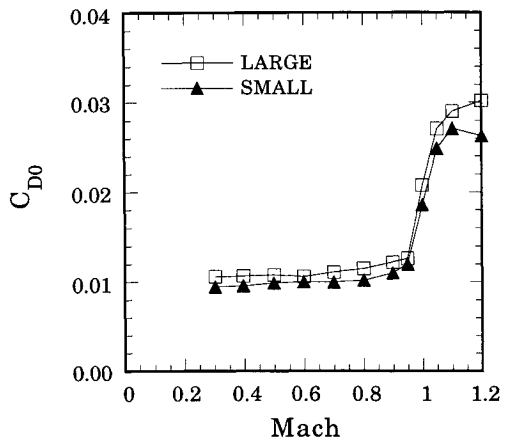

Fig. 9 Zero-lift drag vs Mach number.

Conclusions

The use of different scale models, operating in a given wind tunnel under identical flow conditions, appears to be an appropriate procedure to gain information on wall interference effects; in fact, this approach abolishes any differences related to different flow conditions, and the uncertainty in measurement comparisons is considerably reduced, being limited to the random component (which can be reduced, theoretically, to any desired values), of the measurement procedure as well as to the bias uncertainty related to balances.

The present research activity addressed wall interference effects on longitudinal aerodynamic characteristics, especially as related to pressure-dependent forces. An accurate analysis of the zero-lift drag would actually require a specialized test campaign, with an appropriate choice of instruments and testing techniques.

The test section geometry is very close to that generally suggested as the design producing a wall interference-free environment for moderately sized models (such as the large model used here). The results presented in this article would confirm that this solution is able to significantly reduce wall interference effects, particularly in the very critical conditions of Mach numbers close to 1.

However, in some flow conditions, despite the moderate dimensions of the large model, wall interference effects are probably present. In particular, the pressure-dependent forces appear to be affected by blockage effects at high angles of attack in the low transonic regime ($M \approx 0.7$–0.95). However, since blockage effects on pressure actions were likely to be caused by the same factors, they tended to disappear when longitudinal stability and lift-dependent drag were studied as a function of lift characteristics. This is for the tailless configurations like the tested one; the extension to a complete configuration is not necessarily immediate.

Another parameter that may be considered affected by blockage effects is the zero-lift drag in the supersonic regime, although no definite conclusions can be reached in the subsonic regime, since the measurement procedure adopted is not sufficiently accurate for evaluating the zero-lift drag. However, it should be observed that the drag rise Mach number evaluation appears to be free of blockage effects, even though the large error in the measurement of the zero-lift drag does completely grant this.

These conclusions cannot be immediately extended to different configuration types, it being difficult to generalize wall-interference results from any one configuration. However, it is possible to indicate that when a model with dimensions comparable with the large one is utilized in a test section like the one used here (which is typical for the latest transonic wind tunnels), it can probably be considered not affected by significant blockage effects (with respect to lift characteristics and not to the angles of attack). It appears that the above dimensions should be considered the largest acceptable for corrected industrial applications, even though they are probably not sufficiently small if high accuracy is required.

It must be noted that the principle objective of this work was to analyze the global blockage effects, therefore, no correction procedure was taken into consideration, and the results thus achieved are not the "best" obtainable in the tunnel. By applying the classic corrections a significant increase in the accuracy of the results can be expected; improvement in the accuracy can also be achieved by testing the models in a "redefined" test space, where the offset calibration parameter $(\bar{M} - M_P)$ is re-evaluated for each applicable test space with every different model installation, thereby granting minimal bias.

References

[1]Vayssaire, J. C., "Survey of Methods for Correcting Wall Constraints in Transonic Wind Tunnels," Problems in Wind Tunnel Testing Techniques, AGARD Rept. 601, April 1973.

[2]Bengelink, R. L., and Zinserling, N. J., "Wall Interference Measurements for Three-Dimensional Models in Transonic Wind Tunnels: Experimental Difficulties," NASA CP 2319, Jan. 1983.

[3]Ashill, P. R., "Boundary-Flow Measurements Methods for Wall Interference Assessment and Correction—Classification and Review," 73rd AGARD Fluid Dynamics Panel Meeting and Symposium on Wall Interference, Support Interference and Flow Field Measurements, Brussels, Belgium, Oct. 1993.

[4]Ferri, A., and Baronti, P., "A Method for Transonic Wind-Tunnel Corrections," *AIAA Journal*, Vol. 11, No. 1, 1973, pp. 63–66.

[5]Monti, R., "Wall Corrections for Airplanes with Lift in Transonic Wind Tunnel Tests," AGARD Ad Hoc Committee on Engine—Airplane Interference and Wall Corrections in Transonic Wind-Tunnel Tests, AGARD AR 36, Aug. 1971.

[6]Vaucheret, X., and Vayssaire, J. C., "Corrections de Parois en Ecoulement Tridimensionnel Transsonique dans des Veines a Parois Ventilées," 73rd AGARD Fluid Dynamics Panel Meeting and Symposium on Wall Interference, Support Interference and Flow Field Measurements, Brussels, Belgium, Oct. 1993.

[7]"Specification for the AGARD Wind Tunnel Calibration Models," AGARD Memorandum AG-4/M3, Aug. 1955.

[8]Hills, R. (ed.), "A Review of Measurements on AGARD Calibration Models," AGARDograph 64, Nov. 1961.

[9]Ongarato, J. R., "Wind-Tunnel Wall Interference Studies at High Subsonic Speeds," *Journal of Aircraft*, Vol. 6, No. 2, 1969, pp. 144–149.

[10]Otto, H., "Systematical Investigations of the Influence of Wind-Tunnel Turbulence on the Results of Model Force-Measurements," Wind Tunnel Design and Testing Techniques, AGARD CP 174, Oct. 1975.

[11]Anderson, C. F., "An Investigation of the Aerodynamic Characteristics of the AGARD Model B for Mach numbers from 0.2 to 1.0," Arnold Engineering Development Center, AEDC-TR-70-100, May 1970.

[12]Hurlin, R. S., and Davis, M. W., "Preliminary Calibration Results for the CSIR Medium Speed Wind Tunnel," DAST Rept. 90-320, CSIR, Pretoria, South Africa, Nov. 1990.

[13]Martindale, W. R., "The CSIR Medium Speed Wind Tunnel-Automation for High Productivity with Excellent Flow Quality," Sverdrup Projects 9259, CSIR, Pretoria, South Africa, Dec. 1990.

[14]Christison, R., "Dimensional Inspection Report," Projects Expedited (PTY) LTD Calibration Equipment, Book 1, CSIR, Pretoria, South Africa, 1988.

[15]Davis, M. W., "Analysis of Pressure Measurement Error as Applied to the Static-Pipe Calibration of MSWT," 26th Subsonic Aerodynamic Testing Association, Torino, Italy, May 1990.

[16]Lombardi, G., and Morelli, M., "Wind-Tunnel Blockage Effects on the AGARD B Model in Transonic Flow," 19th Congress of the International Council of the Aeronautical Sciences, Anaheim, CA, Sept. 1994.

[17]Coleman, H. W., and Steele, W. G., "Experimentation and Uncertainty Analysis for Engineers," Wiley, New York, 1989.